photonics

MDPI

Article

Suppression of Bottom Porosity in Fiber Laser Butt Welding of Stainless Steel

Xiaobing Pang [1,*], Jiahui Dai [2], Mingjun Zhang [2] and Yan Zhang [3]

[1] College of Mechanical & Electrical Engineering, Changsha University, Changsha 410022, China
[2] Key Laboratory of High Performance Intelligent Manufacturing of Mechanical Equipment of Hunan Province, Changsha University of Science & Technology, Changsha 410114, China; daijiahui2018@163.com (J.D.); mj_zhang@csust.edu.cn (M.Z.)
[3] Hunan Institute of Science and Technology, College of Mechanical Engineering, Yueyang 414006, China; 12017032@hnist.edu.cn
* Correspondence: pangxiaobing55@ccsu.edu.cn; Tel./Fax: +86-731-8426-1492

Abstract: The application bottleneck of laser welding is being gradually highlighted due to a high prevalence of porosity. Although laser welding technology has been well applied in fields such as vehicle body manufacturing, the suppression of weld porosity in the laser welding of stainless steel containers in the pharmaceutical industry is still challenging. The suppression of bottom porosity was investigated by applying ultrasonic vibration, changing welding positions and optimizing shielding gas in this paper. The results indicate that bottom porosities can be suppressed through application of ultrasonic vibration at an appropriate power. The keyhole in ultrasound-assisted laser welding is easier to penetrate, with better stability. No obvious bulge at the keyhole rear wall is found in vertical down welding, and the keyhole is much more stable than that in flat welding, thus eliminating bottom porosity. The top and bottom shielding gases achieve the minimal total porosities, without bottom porosity.

Keywords: fiber-laser welding; porosity; suppression; stainless steel

Citation: Pang, X.; Dai, J.; Zhang, M.; Zhang, Y. Suppression of Bottom Porosity in Fiber Laser Butt Welding of Stainless Steel. *Photonics* **2021**, *8*, 359. https://doi.org/10.3390/photonics8090359

Received: 8 June 2021
Accepted: 26 August 2021
Published: 28 August 2021

1. Introduction

304 austenitic stainless steel, due to its good corrosion resistance and mechanical properties, has been widely used in fields including pressure vessels and nuclear power equipment [1]. Argon tungsten arc welding (TIG) is currently dominant in manufacturing plates of isolators and freeze-dryers in the pharmaceutical field. However, this traditional arc welding method is associated with some disadvantages such as limited penetration ability, low welding efficiency and poor controllability of heat input [2]. Laser welding is expected to be feasible for welding stainless-steel containers in the pharmaceutical field due to its high energy density, high welding speed and small deformation after welding. However, it is susceptible to porosities, especially the bottom porosities as a result of the instability of the deep-penetration keyhole, which affects the sealing and anti-pollution ability of the weld seam and restricts its application in welding pharmaceutical containers [3]. Therefore, it is of great significance to suppress bottom porosities in laser welding of stainless steel for the application of laser welding technology in pharmaceutical container manufacturing.

Considering porosity as a common defect in a laser-welded seam and the lack of systematic control theoretical basis, laser welding technology is gradually reaching its application bottleneck [4,5]. Process-induced porosity is the hotspot in research on the porosity of laser welding, mainly including keyhole-induced porosity [6,7] and fluid-flow-induced porosity [8,9]. Lin et al. [6] found in a numerical simulation that the formation of bubbles in the weld pool of remote laser welding of aluminum alloy depends on the dynamic behaviors of the keyhole and weld pool. Specifically, the collapse of the keyhole

caused by an intense melt flow and the eddy along the weld pool behind the keyhole are the main contributors to the formation of bubbles. Based on a high-speed photography analysis during the weld test of glass and metal composite specimens, Xu et al. [7] argued that the sharp fluctuation of the keyhole may explain to a great extent the formation and assemblage of bubbles, which resulted in large porosities. Zhang et al. [10] compared the porosity defects of non-penetration and full-penetration laser welding by numerical simulation combined with intuitive observation and revealed that full-penetration laser welding greatly improved the porosity defects and that the formation mechanism of porosity in full-penetration laser welding was consistent with the "hump theory" [11]. Meng et al. [8] studied the formation mechanism of porosity at the T-joint of laser lap welding and proposed that the change of dynamic behaviors of the weld pool is the main reason for the formation of porosities at the lap gap, while the instability of the keyhole is insignificant in laser lap welding. Panwisawas et al. [9] showed that process-induced porosity is related to plate thickness, laser power and welding speed in laser welding of titanium alloy plates. Especially, the porosity increases with the increase of plate thickness. Meanwhile, it is pointed out that unstable flow and/or porosity escape time relative to local solidification time is the key to porosity formation.

Numerous research studies have been conducted on the suppression of porosity in laser welding, with many methods proposed, such as pulsed laser welding [12], laser-beam oscillation scanning welding [13,14], ultrasound-assisted laser welding [15,16], changing welding position [17,18] and optimizing shielding gas [19,20]. Shen et al. [12] examined the effects of laser pulse parameters on porosity and flow characteristics of the weld pool and exhibited a negative correlation between pulse frequency and porosity at the joint and the suppression mechanism of porosity in pulsed laser welding. That is, pulsed laser welding results in good stability of the keyhole and limits bubble formation by preventing shielding gas from being involved in the keyhole. Meanwhile, the intermittent impact effect of pulsed laser accelerates the escape of bubbles by stirring the weld pool, thus further reducing porosities. Zhou et al. [13] discovered by utilization of the beam oscillation scanning method in laser welding of aluminum alloy that circular scan is effective in eliminating porosities. Furthermore, improvement in the stability of the keyhole was established as the main reason for the elimination of porosities by recording the fluctuation degree of the entrance of the keyhole during laser beam scanning. Cai et al. [14] explored the swing laser-MAG hybrid welding of carbon steel and pointed out that the swing laser changes the root shape of the hybrid weld seam, facilitating elimination of root porosity. Kim et al. [15] first proposed the use of ultrasonic vibration on the bottom of the specimen during laser welding. It was demonstrated that cracks and porosities in the weld seam are greatly suppressed by the ultrasonic vibration due to cavitation effects in the molten pool during ultrasound-assisted laser welding. Lei et al. [16] suggested that the porosity at the weld seam is greatly improved by the cavitation and acoustic streaming of the ultrasonic vibration on the weld pool in ultrasound-assisted laser welding of AZ31B magnesium alloy. Grajczak et al. [21] found that porosity can be eliminated when the weld pool is located in the antinode position during ultrasound-assisted laser welding of nickel-based-alloy round bars. He and Shen [17] analyzed the effects of different welding positions on porosity in laser welding of aluminum alloys and observed the minimal porosities in vertical down welding, with high stability of the keyhole. Miao et al. [18] noted that the number of porosities in vertical welding is smaller than that in flat welding. He and Shen [19] proved that porosity is significantly decreased by the addition of side-blowing gas flow in laser welding of aluminum alloy and that the flow rate has a great influence on porosity. Sun et al. [20] determined that when nitrogen (N2) is used as shielding gas in laser welding of 304 stainless steel, porosity is suppressed and is mainly seen at the bottom of the weld seam. The solubility of N2 in the liquid weld pool contributes to reducing the porosity in laser welding of 304 stainless steel.

In conclusion, abundant studies focus on porosity defects in the laser welding process, and the formation mechanism and suppression methods of porosity have been extensively

validated. However, there are few reports on bottom porosity. The suppression of bottom porosity was investigated by applying ultrasonic vibration, changing welding positions and optimizing shielding gas during laser welding of 304 stainless steel in this paper, and the suppression mechanisms of porosity caused by ultrasonic vibration, welding position and shielding gas were revealed by observation of the dynamic laser welding process with high-speed photography.

2. Experimental Procedure

The experimental setup was as illustrated in Figure 1. With a continuous-wave fiber laser (YLS-3000-CL) as the laser source, the laser beam emitted from the end of the operation fiber was collimated and then focused with the aid of a laser welding head (FLW-D30), while for the laser beam radiated from the end of the optical fiber, collimation was conducted by a lens of a 100 mm focal length, and focusing on the specimen surface was completed by a focusing unit of a 150 mm focal length. After focusing, the laser beam had a spot size of about 0.3 mm. The ultrasonic power supply (CSHJ-1000) that has an ultrasonic frequency of 20 kHz was applied to provide the power output of 1000 W with a fixed amplitude of 6 μm. The ultrasonic amplitude transformer was placed in a sink on the working platform. The configuration of the bead-on-plate welding with ultrasound is illustrated in Figure 1c.

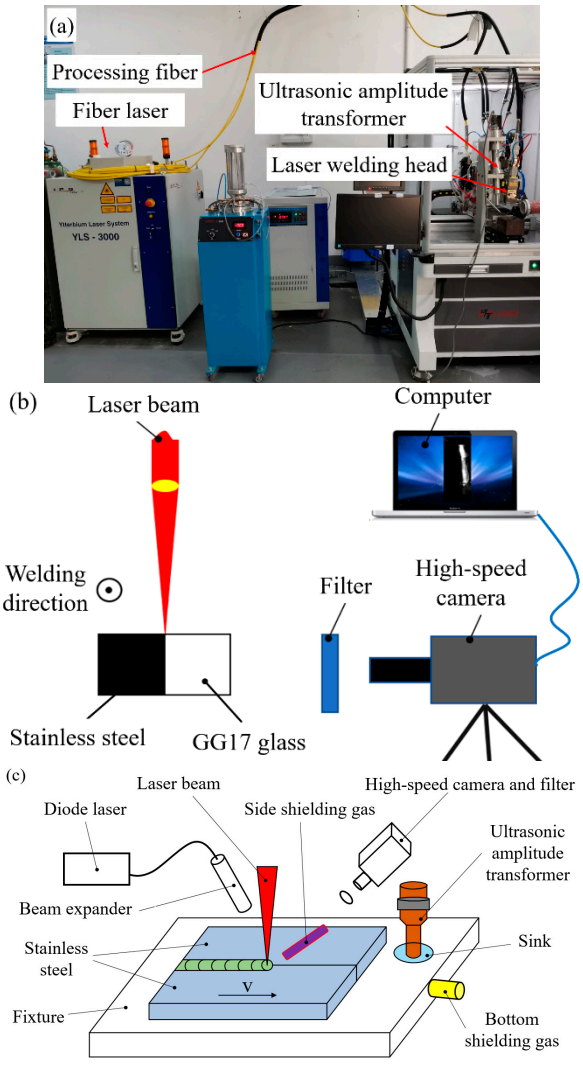

Figure 1. Experimental setup: (**a**) on-site layout, (**b**) schematic diagram of welding with "sandwich" specimen and (**c**) schematic diagram of bead-on-plate welding with ultrasound.

The welding materials used were 304 stainless steel plates of 3 mm in thickness. Table 1 overviews the substrate with respect to its chemical composition. The modified sandwich sample comprises, as displayed in Figure 1b, one sheet of stainless steel and one sheet of GG17 glass, both with a size of 50 mm × 3 mm × 3 mm [22]. The processing parameters for the laser welding experiments are presented in Table 2.

Table 1. Chemical composition of the 304 stainless steel studied.

Element	C	Cr	Mn	Ni	Si	P	S	Fe
(Wt.%)	0.039	18.280	1.420	8.150	0.410	0.036	0.015	Bal.

Table 2. Parameters used in the welding experiments.

Parameters	Value
Laser power (p_{laser}) (W)	2000
Welding speed (v) (m/min)	1.2
Defocus (Δ) (mm)	+3
Ultrasonic frequency (kHz)	20
Ultrasonic power ($p_{ultrasonic}$) (W)	0, 250, 500, 750, 1000
Ultrasonic amplitude (μm)	6
Welding position	Flat position, Vertical–down position, Vertical–up position, Horizontal position
Shielding gas type	N_2
Top shielding gas flow rate (q_{top}) (L/min)	0, 15, 20, 25
Bottom shielding gas flow rate (q_{bottom}) (L/min)	0, 15, 20, 25

The welding zone was illuminated by a diode laser (808 nm) with a maximum power of 30 W for general observation of the weld pool, and for selective observation, a filter was additionally added to the camera lens. To visualize the weld pool and the vapor plume during the experiments, a bandpass filter with a transmission band of 808 ± 3 nm and a filter with a transmission band from 350 nm to 650 nm were placed in front of the camera lens, respectively.

An X-ray real-time imaging system (XYD-225) was used to detect the pores in the welding test piece upon completion of welding. After being cut by electro-discharge machining (EDM), the longitudinal sections of the welded joints were polished with abrasive paper and polishing cloth. The finished cross sections of the welded joints were observed under an optical microscope (Leica S9i) upon etching by a solution of aqua regia ($HCl:HNO_3$ = 3:1) for 15 s.

3. Results and Discussion

3.1. Effect of Ultrasonic Vibration on Bottom Porosity

The X-ray nondestructive inspection and longitudinal sectional view of weld seams at different ultrasonic powers are shown in Figure 2. The parameters of laser welding included the laser power of 2000 W, welding speed of 20 mm/s and defocus of +3 mm. Nitrogen was used as the shielding gas, with the flow rate of 20 L/min, the angle of 30° between the shielding gas nozzle and laser beam and the ultrasonic power of 0, 250 W, 500 W, 750 W and 1000 W. Bottom porosities are defined as those located within the depth of 1 mm at the bottom of the weld seam. Figure 2 indicates the maximal total porosities are obtained without ultrasonic vibration, as shown by the blue arrows in Figure 2. The porosities are distributed at the upper, middle and lower parts of the weld seam, with three bottom porosities, as shown by the red arrows in Figure 2. The total and bottom porosities both decrease at the ultrasonic power of 250 W and 500 W. The most significant suppression with one pore in total is achieved as the ultrasonic power increases to 750 W. Only a few pores are observed near the upper surface of the weld seam, without bottom porosities. When the ultrasonic power continues to increase to 1000 W, the total number of

porosities increases to four. The porosities are found at the middle and upper part of the weld seam, without bottom porosities. Therefore, it can be concluded that the potential of having fewer porosities is obtained by the application of ultrasonic vibration with a critical value of ultrasonic power.

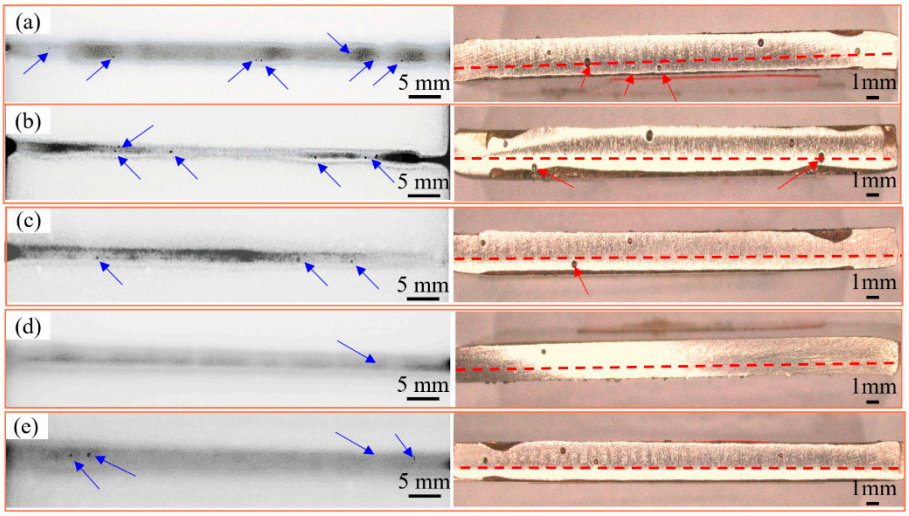

Figure 2. Distribution of porosities at different ultrasonic powers: (**a**) 0, (**b**)250 W, (**c**) 500 W, (**d**) 750 W, (**e**) 1000 W.

The dynamic change process of the keyhole and weld pool in conventional laser welding of "sandwich" specimens is presented in Figure 3. The shape of the keyhole is normal, without obvious fluctuation at t = 0.994 s (Figure 3a). After a short while, a local bulge is observed at the bottom of the keyhole's rear wall (Figure 3b). Subsequently, the brightness inside the keyhole increases sharply, with an obvious local bulge in the middle part of the keyhole's rear wall, and the entrance at the bottom of the keyhole narrows and necks down (Figure 3c). Soon afterward, a local bulge in the middle part of the keyhole's rear wall continues to enlarge, with necking down at the bottom of the keyhole (Figure 3d). Since the local bulge in the middle part of the keyhole's rear wall enlarges, and more importantly, the bottom of the keyhole necks down and gradually folds, an independent bubble is formed, as shown in Figure 3e,f. As the welding process progresses, the keyhole develops downward and finally fuses with the bubble (Figure 3g), whereafter the local bulge in the middle part of the keyhole's rear wall becomes smaller (Figure 3h). The brightness inside the keyhole increases (Figure 3i), with a local bulge in the middle part of the keyhole's front wall and shrinkage of the bottom of the keyhole at t + 2. 4 ms (see Figures 3j and 3k, respectively).

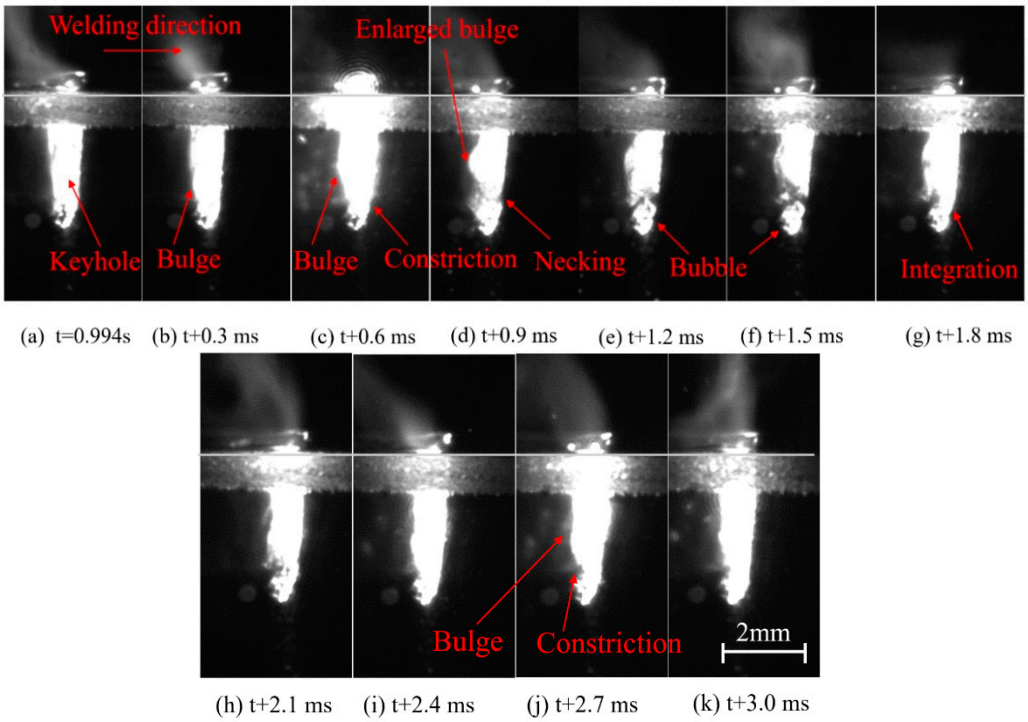

Figure 3. Dynamic change process of the keyhole and weld pool in conventional laser welding of "sandwich" specimen (p_{laser} = 2000 W, v = 1.2 m/min, Δ = +3 mm, q_{top} = 20 L/min (N_2)).

The dynamic change process of the keyhole and weld pool in ultrasound-assisted laser welding of "sandwich" specimens is provided in Figure 4. An obvious bulge is observed at the keyhole's rear wall, with a narrow outlet of the keyhole at t = 0. 339 s (Figure 4a). The brightness inside the keyhole increases sharply, and the keyhole elongates downward, with a smaller bulge in the keyhole's rear wall at t + 0. 3 ms (Figure 4b). Subsequently, the outlet of the keyhole opens, with the molten metal spraying downward and the diminution of the keyhole (Figure 3c). At this moment, the keyhole is prone to collapse, since the steam pressure inside it drops significantly (Figure 4d). Hereafter, a new keyhole is formed under the action of continuous laser-beam energy, and the newly formed keyhole is bright (indicating relatively concentrated energy inside) and gradually moves down (Figures 4d and 4e, respectively). As the welding process progresses, the newly formed keyhole develops downward and fuses with the collapsed one, with an obvious local bulge at the rear wall of the fused keyhole (Figure 4f). Afterward, the outlet of the keyhole opens, with the molten metal spraying downward and the disappearance of the local bulge at the keyhole's rear wall (Figure 4g).

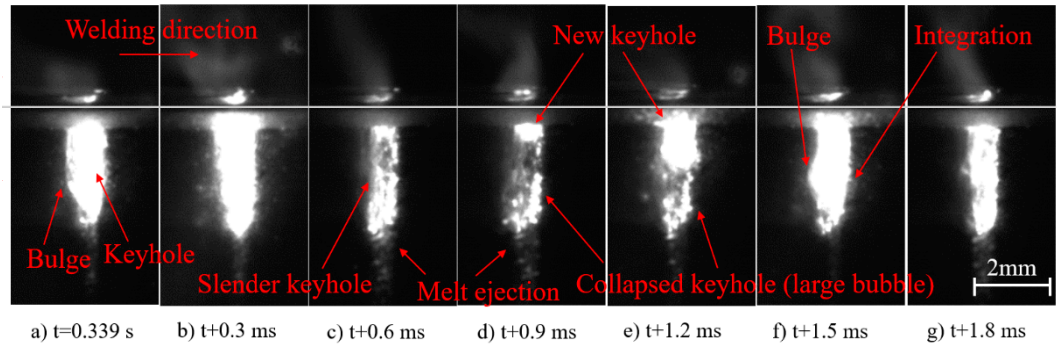

Figure 4. Dynamic change process of the keyhole and weld pool in ultrasound-assisted laser welding of "sandwich" specimen (p_{laser} = 2000 W, v = 1.2 m/min, Δ = +3 mm, $p_{ultrasonic}$ = 750 W, q_{top} = 20 L/min (N_2)).

To sum up, the keyhole's rear wall is always subject to fluctuation in conventional laser welding, especially, the bottom of which is prone to local bulges; moreover, poor stability of the bottom of the keyhole can easily lead to necking down of the bottom and further cause bubbles, thus forming keyhole-induced porosity [6,7]. Under the same welding parameters, the keyhole in ultrasound-assisted laser welding is easier to penetrate, with less local bulging and longer time of stability maintaining at the keyhole's rear wall, compared with conventional laser welding. Despite the collapse, the formation of the new keyhole is relatively stable. Local bulging at the keyhole's rear wall is often accompanied by the penetration of the bottom of the keyhole to ensure its stability.

3.2. Effect of Welding Position on Bottom Porosity

The X-ray nondestructive inspection and longitudinal sectional view of weld seams at different welding positions are displayed in Figure 5. The porosities in the X-ray nondestructive inspection and the bottom porosities in the longitudinal section are shown by the blue and red arrows, respectively. As indicated in Figure 5, the total number of porosities declines in horizontal position welding, vertical up welding and vertical down welding, compared with flat welding (Figure 2a). Among them, the largest total number of porosities is obtained in vertical up welding, with some bottom porosities (Figure 5a). The optimum suppression of porosities is achieved in vertical down welding, without bottom porosities (Figure 5b). The porosities in horizontal position welding are fewer than those in flat welding, as indicated in Figure 5c. The results indicate that the potential of having fewer porosities is achieved with the welding position of vertical down welding.

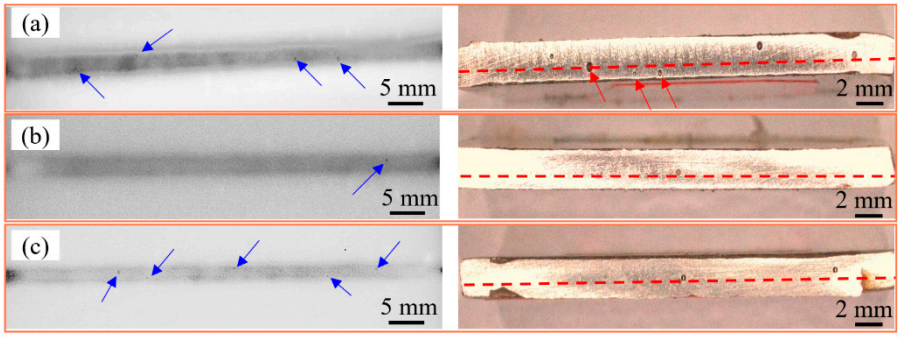

Figure 5. Distribution of porosities at different welding positions: (**a**) vertical up welding, (**b**) vertical down welding and (**c**) horizontal position welding.

The dynamic change process of the keyhole and weld pool in vertical down laser welding of "sandwich" specimens is given in Figure 6. As shown in Figure 6, the fluctuation of the keyhole in vertical down laser welding is smaller than that in conventional laser welding. The shape of the keyhole is stable with great brightness inside at t = 0. 147 s (Figure 6a). Subsequently, the bottom of the keyhole necks down and collapses successively (Figure 6b,c). Soon afterward, the keyhole moves deep to the bottom again, with a complete new keyhole formed (Figure 6d,e). With the progress of welding, laser energy accumulation is found successively at the middle and middle-upper parts of the keyhole, accompanied by a local bulge in the keyhole's rear wall but without collapse, as demonstrated in Figure 6f–j.

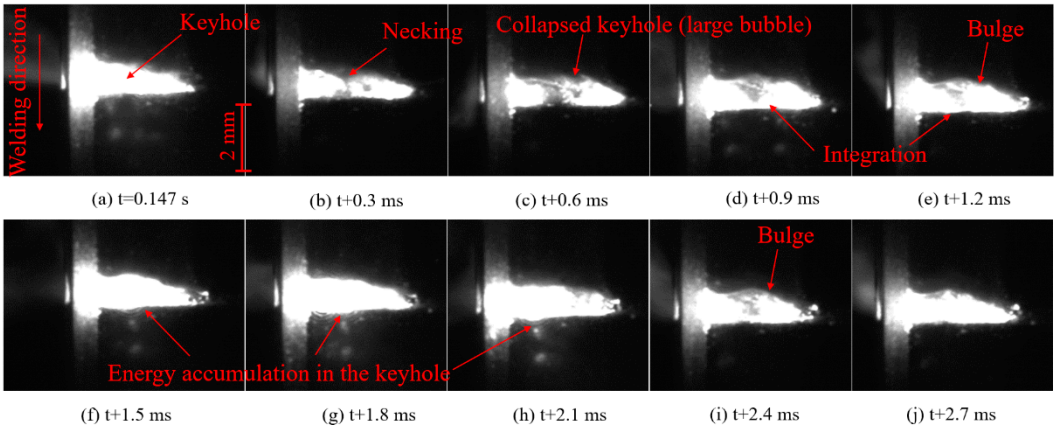

Figure 6. Dynamic change process of the keyhole and weld pool in vertical down laser welding of "sandwich" specimen (p_{laser} = 2000 W, v = 1.2 m/min, Δ = +3 mm, q_{top} = 20 L/min (N_2)).

In summary, no obvious bulge at the keyhole's rear wall is found in vertical down welding, and its keyhole is more stable than that in flat welding, which thus diminishes the formation of keyhole-induced porosity at its source. Moreover, compared with flat welding, the force direction on its weld pool along the welding direction is consistent with the gravity, and thus the weld pool is lengthened, and the escape time of bubbles is prolonged [17]. Therefore, the number of porosities, especially that of bottom porosities, is greatly reduced.

3.3. Effect of Shielding Gas on Bottom Porosity

The effects of flow rate and supply method of shielding gas on the total and bottom porosities are illustrated in Figure 7. The highest number of total and bottom porosities is caused when only top shielding gas is applied, as shown in Figures 7a and 7b, respectively. Compared with top shielding gas alone, the total and bottom porosities both decrease when only bottom shielding gas is applied, as shown in Figures 7a and 7b, respectively. The lowest number of total and bottom porosities is found when the top and bottom shielding gases are both applied, as shown in Figures 7a and 7b, respectively. No bottom porosity is formed occasionally at the flow rate of 20 L/min, as shown in Figure 7b. The results indicate that the potential of having fewer porosities is obtained when the top and bottom shielding gases are both applied with a moderate flow rate.

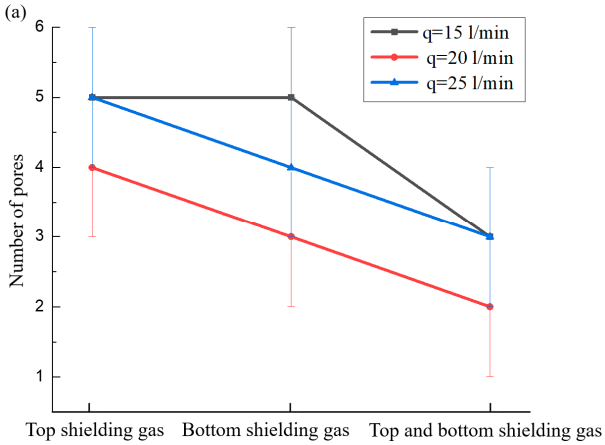

Figure 7. *Cont.*

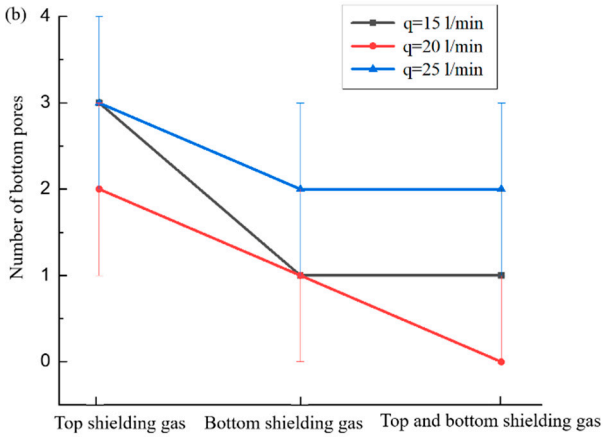

Figure 7. Effects of flow rate and supply method of shielding gas on the number of porosities.

The high-speed photograph of the upper-surface weld pool and entrance of the keyhole during laser welding without shielding gas is demonstrated in Figure 8. Figure 9 provides the high-speed photograph of the upper-surface weld pool and entrance of the keyhole when top and bottom shielding gases are applied simultaneously. As indicated in Figure 8, without shielding gas, the length of the upper-surface weld pool is about 4.0 mm, with a width of about 2.1 mm, and the opening and closing cycle of the entrance of the keyhole is about 2.4 ms during laser welding. The length of the upper-surface weld pool is about 7.2 mm, with a width of about 2.6 mm, and the opening and closing cycle of the entrance of the keyhole is about 5.1 ms, when top and bottom shielding gases are applied simultaneously. Compared to the case without shielding gas, the length and width of the upper-surface weld both increase, with the stability-maintaining time of the entrance of the keyhole prolonged, when top and bottom shielding gases are applied simultaneously. Therefore, the increase in the volume of the weld pool and improvement in the stability of the keyhole guarantee fewer bubbles caused by the collapse of the keyhole, when top and bottom shielding gases are applied simultaneously. Despite the bubbles formed, the larger weld pool provides the bubbles with a longer time to escape upward, and thus the porosity defects at the bottom of the weld seam are better improved.

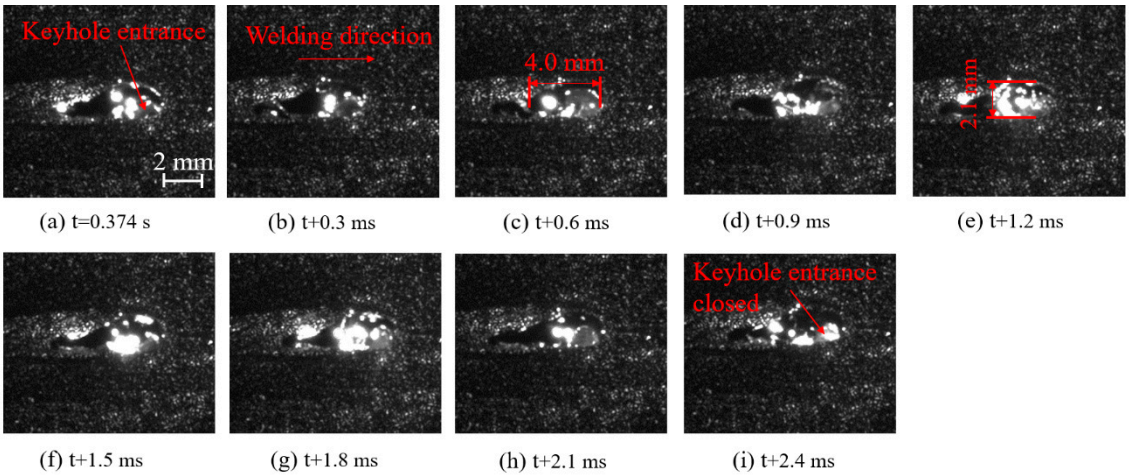

Figure 8. Dynamic change process of the weld pool and keyhole entrance during laser welding without shielding gas (p_{laser} = 2000 W, v = 1.2 m/min, Δ = +3 mm).

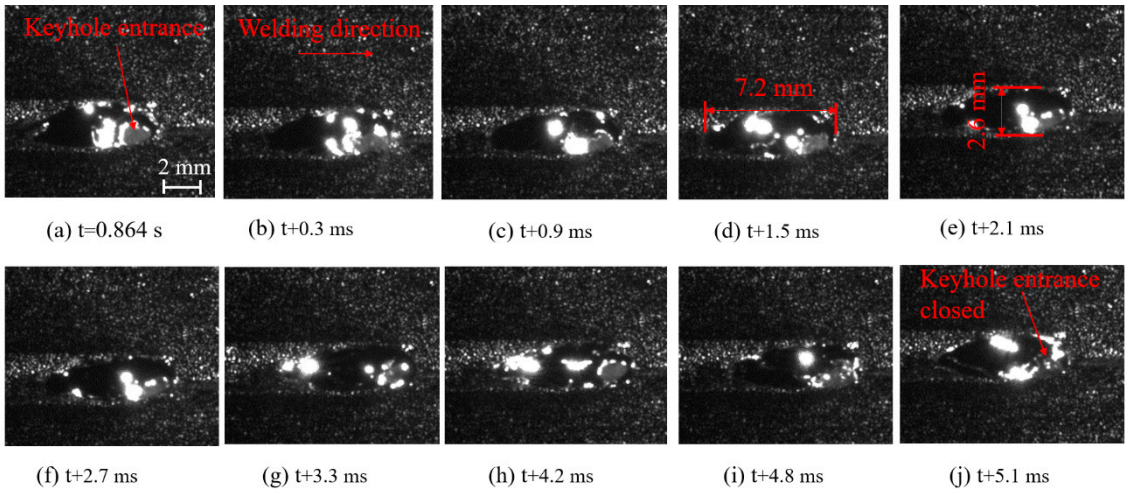

Figure 9. Dynamic change process of the weld pool and keyhole entrance during laser welding with both top and bottom shielding gases (p_{laser} = 2000 W, v = 1.2 m/min, Δ = +3 mm, q_{top} = 20 L/min (N_2), q_{bottom} = 20 L/min (N_2)).

4. Conclusions

Given the limited reports on suppression of the porosity defect in the fiber-laser welding stainless steel, laser welding experiments were conducted on 304 stainless steel specimens by applying ultrasonic vibration, changing welding position and optimizing shielding gas. With a combination of processing experiments and high-speed photography observation of the welding process, the porosity, especially the bottom porosity defects in the weld, was analyzed. The following conclusions were made based on the experiments.

(1) The potential of having fewer porosities occurs when the ultrasonic vibration is applied with a critical value of ultrasonic power. Compared with conventional laser welding, the welding keyhole in ultrasound-assisted laser welding is easier to penetrate, with less local bulging and longer time of stability maintaining at the keyhole rear wall, thus leading to reduced porosities.

(2) Welding position exerts a great influence on porosity formation in laser welding. The optimal suppression of porosities is achieved in vertical down welding, followed by horizontal position welding. No obvious bulge at the keyhole's rear wall is observed in vertical down welding, and the keyhole is more stable than that in flat welding, thus suppressing porosities.

(3) The potential of having fewer porosities is obtained when the top and bottom shielding gases are both applied with a moderate flow rate. When top and bottom shielding gases are applied simultaneously, the length and width of the weld pool increase, with good stability of the entrance of the keyhole, thus facilitating porosity reduction.

Author Contributions: Conceptualization, X.P.; methodology, X.P.; software, X.P.; validation, M.Z. and Y.Z.; formal analysis, X.P.; investigation, X.P. and J.D.; resources, X.P.; data curation, X.P.; writing—original draft preparation, X.P. and J.D.; writing—review and editing, Y.Z.; visualization, Y.Z.; supervision, Y.Z.; project administration, M.Z. and Y.Z.; funding acquisition, M.Z. and Y.Z. All authors have read and agreed to the published version of the manuscript.

Funding: The authors are grateful for the financial support from the National Natural Science Foundation of China (No. 51605045, 51875050), the Natural Science Foundation of Hunan Province of China (No. 2021JJ30302), and the Science and Technology Plan Project of Changsha City (No. kq1907089).

Institutional Review Board Statement: This study did not involve humans or animals.

Informed Consent Statement: Not applicable.

Data Availability Statement: This study does not report any data.

Conflicts of Interest: The authors declare no conflict of interest.

References

1. Zhang, M.; Chen, S.; Zhang, Y.; Chen, G.; Bi, Z. Mechanisms for improvement of weld appearance in autogenous fiber laser welding of thick stainless steels. *Metals* **2018**, *8*, 625. [CrossRef]
2. Cheng, Z.; Liu, H.; Huang, J.; Ye, Z.; Yang, J.; Chen, S. MIG-TIG double-sided arc welding of copper-stainless steel using different filler metals. *J. Manuf. Process.* **2020**, *55*, 208–219. [CrossRef]
3. Zhang, L.; Zhang, J.; Zhang, G.; Bo, W.; Gong, S. An investigation on the effects of side assisting gas flow and metallic vapour jet on the stability of keyhole and molten pool during laser full-penetration welding. *J. Phys. D Appl. Phys.* **2011**, *44*, 135201. [CrossRef]
4. Chen, D.; Zhan, X.; Liu, T.; Zhao, Y.; Qi, N.; Sun, L. Effect of porosity morphology and elements characteristics on mechanical property in T-joints during dual laser-beam bilateral synchronous welding of 2060/2099 Al-Li alloys. *Opt. Laser Technol.* **2021**, *140*, 107019. [CrossRef]
5. Shi, L.; Li, X.; Jiang, L.; Gao, M. Numerical study of keyhole-induced porosity suppression mechanism in laser welding with beam oscillation. *Sci. Technol. Weld. Join.* **2021**, *26*, 349–355. [CrossRef]
6. Lin, R.; Wang, H.; Lu, F.; Solomon, J.; Carlson, B.E. Numerical study of keyhole dynamics and keyhole-induced porosity formation in remote laser welding of Al alloys. *Int. J. Heat Mass Transf.* **2017**, *108*, 244–256. [CrossRef]
7. Xu, J.; Rong, Y.; Huang, Y.; Wang, P.; Wang, C. Keyhole-induced porosity formation during laser welding. *J. Manuf. Process.* **2018**, *252*, 720–727. [CrossRef]
8. Meng, W.; Li, Z.; Lu, F.; Wu, Y.; Chen, J.; Katayama, S. Porosity formation mechanism and its prevention in laser lap welding for T-joints. *J. Manuf. Process.* **2014**, *214*, 1658–1664. [CrossRef]
9. Panwisawas, C.; Perumal, B.; Ward, R.M.; Turner, N.; Turner, R.P.; Brooks, J.W.; Basoalto, H.C. Keyhole formation and thermal fluid flow-induced porosity during laser fusion welding in titanium alloys: Experimental and modelling. *Acta Mater.* **2017**, *126*, 251–263. [CrossRef]
10. Zhang, R.; Tang, X.; Xu, L.; Lu, F.; Cui, H. Study of molten pool dynamics and porosity formation mechanism in full penetration fiber laser welding of Al-alloy. *Int. J. Heat Mass Transf.* **2020**, *148*, 119089. [CrossRef]
11. Matsunawa, A.; Mizutani, M.; Katayama, S.; Seto, N. Porosity formation mechanism and its prevention in laser welding. *Weld. Int.* **2003**, *17*, 431–437. [CrossRef]
12. Shen, X.; Zhao, S.; Teng, W.; He, W. Effects of pulse parameters on porosity rate and flow characteristics of molten pool in pulsed laser welding. *J. Laser Appl.* **2018**, *30*, 32405. [CrossRef]
13. Zhou, L.T.; Wang, X.Y.; Wang, W.; Wang, S.Y. Effects of laser scanning welding process on porosity rate of aluminum alloy. *Trans. China Weld. Inst.* **2014**, *35*, 65–68.
14. Cai, C.; Li, L.; Tao, W.; Chen, X. Effects of weaving laser on scanning laser-MAG hybrid welding characteristics of high-strength steel. *Sci. Technol. Weld. Join.* **2017**, *22*, 104–109. [CrossRef]
15. Kim, J.S.; Watanabe, T.; Yoshida, Y. Ultrasonic vibration aided laser welding of Al alloys: Improvement of laser welding-quality. *J. Laser Appl.* **1995**, *7*, 38–46. [CrossRef]
16. Lei, Z.; Bi, J.; Li, P.; Guo, T.; Zhao, Y.; Zhang, D. Analysis on welding characteristics of ultrasonic assisted laser welding of AZ31B magnesium alloy. *Opt. Laser Technol.* **2018**, *105*, 15–22. [CrossRef]
17. He, W.P.; Shen, X.F. Effects of welding position on welding quality in CO_2 laser welding of 5A90 aluminum-lithium alloy. *High Power Laser Part. Beams* **2016**, *28*, 178–186.
18. Miao, Y.G.; Chen, Y.B.; Li, L.Q.; Wu, L. Analysis of characteristic of vertical position laser welding for aluminum alloys. *Trans. China Weld. Inst.* **2007**, *28*, 57–60.
19. He, W.P.; Shen, X.F. Effect of shielding gas porosity in CO_2 vertical position laser welding of 5A90 aluminum-lithium alloy. *High Power Laser Part. Beams* **2016**, *28*, 14–20.
20. Sun, J.; Nie, P.; Lu, F.; Huang, J.; Feng, K.; Li, Z.; Zhang, W. The characteristics and reduction of porosity in high-power laser welds of thick AISI 304 plate. *Int. J. Adv. Manuf. Technol.* **2017**, *93*, 3517–3530. [CrossRef]
21. Grajczak, J.; Nowroth, C.; Nothdurft, S.; Hermsdorf, J.; Twiefel, J.; Wallaschek, J.; Kaierle, S. Influence of ultrasound on pore and crack formation in laser beam welding of nickel-base alloy round bars. *Metals* **2020**, *10*, 1299. [CrossRef]
22. Zhang, M.; Zhang, Z.; Tang, K.; Mao, C.; Hu, Y.; Chen, G. Analysis of mechanisms of underfill in full penetration laser welding of thick stainless steel with a 10 kW fiber laser. *Opt. Laser Technol.* **2018**, *98*, 97–105. [CrossRef]